Supporting Information

Stabilization of a high H^--conducting phase via K doping of Ba-Li oxyhydride

Kei Okamoto[a,b,c], Fumitaka Takeiri[a,b,c,d], Yumiko Imai[b], Masao Yonemura[e,f], Takashi Saito[e,f], Kazutaka Ikeda[e,f], Toshiya Otomo[e,f], Takashi Kamiyama[e,f], and Genki Kobayashi[a,b,c,*]

[a] Solid State Chemistry Laboratory, Cluster for Pioneering Research (CPR), RIKEN, Wako 351-0198, Japan.

[b] Department of Materials Molecular Science, Institute for Molecular Science, Okazaki 444-8585, Japan.

[c] Department of Structural Molecular Science, School of Physical Sciences, SOKENDAI (The Graduate University for Advanced Studies), Okazaki 444-8585, Japan.

[d] Japan Science and Technology Agency (JST), Precursory Research for Embryonic Science and Technology (PRESTO), 4-1-8 Honcho, Kawaguchi, Saitama 332-0012, Japan.

[e] Institute of Materials Structure Science, High Energy Accelerator Research Organization (KEK), Ibaraki 305-0801, Japan.

[f] Department of Materials Structure Science, School of High Energy Accelerator Science, SOKENDAI (The Graduate University for Advanced Studies), Ibaraki 305-0801, Japan.

* Corresponding author. Genki Kobayashi, Email: genki.kobayashi@riken.jp

Experimental Details

Polycrystalline samples of $Ba_{2-x}K_xLiH_3O$ (x = 0.1, 0.2, or 0.3), denoted as K-BLHO, were synthesized via a high-pressure method using BaH_2 (99.5 %, Mitsuwa Chemical, Amphur Phanthong, Thailand), BaO (99.99%, Sigma-Aldrich, St. Louis, MO, USA), LiH (95%, Sigma-Aldrich), and KH (95%, Sigma-Aldrich) as starting materials. These materials were thoroughly mixed in a stoichiometric ratio via planetary ball-milling in an Ar-filled agate pot for 4 h. The mixture was sealed in a BN sleeve covered with a NaCl capsule inside a pyrophyllite cell in an Ar-filled glovebox. The cell was compressed to a pressure of 2 GPa using a cubic anvil-type press, heated at 400 °C for 30 min, then heated at 650 °C for 30 min, and finally, quenched to room temperature, followed by a slow release of the pressure.

Powder X-ray diffraction (XRD) was performed using a diffractometer (MiniFlex 600, Rigaku, Tokyo, Japan) with CuKα radiation. As the samples were highly air-sensitive, they were loaded into an Al sample holder covered with a Kapton film in an Ar-filled glovebox. Powder synchrotron XRD (SXRD) was performed using the product with x = 0.3 at BL02B2[1] at SPring-8 (Sayo, Japan) with a wavelength of 0.42 Å. The finely ground powder was loaded into a quartz capillary with an inner diameter of 0.3 mm. The sealed capillary was rotated during measurement to reduce the preferred orientations of the crystallites. Temperature-controlled SXRD was measured in the range of 100 to 400 °C at 20 °C intervals, and the collected SXRD profiles were analyzed via the Rietveld method using the RIETAN-FP program.[2]

Time-of-flight neutron diffraction (ND) was conducted using SPICA and NOVA diffractometers at the Japan Proton Accelerator Research Complex (Tokai, Japan). The former is the instrument that combines high intensity and high resolution and is suitable for the refinement of the multiphase analysis, and the latter is the instrument that provides high intensity over a wide-Q range and is capable of high-temperature measurements. For measurements at room temperature, powder samples (~0.2 g) were loaded into the cylindrical vanadium cell (radius = 6 mm, height = 55 mm). For high-temperature measurements, the samples sealed in a quartz tube were loaded into the cell to suppress side reactions with vanadium and sample. The relatively high backgrounds of ND diffraction, especially for high-temperature measurements, are due to the quartz tube and incoherent cross section of hydrogen. The collected ND profiles were analyzed via the Rietveld method using the Z-Rietveld[3] program (High Energy Accelerator Research Organization, Tsukuba, Japan). Crystal structures were visualized using the Visualization for Electronic Structural Analysis program.[4]

The ionic conductivity of K-BLHO (x = 0.3) was determined via alternating current (AC) impedance measurements under H_2 gas at 200–300 °C in an applied frequency range of 0.1 Hz to 35 MHz using an MTZ-35 frequency response analyzer (BioLogic, Seyssinet-Pariset, France). To eliminate the influence of the irreversible α-β transformation, including changes in composition, during measurement, the sample obtained via high-pressure synthesis was annealed at 400 °C for 6 h in a stainless-steel container filled with H_2 gas (0.42 MPa). Ion blocking Mo electrodes were deposited on

both sides of the annealed pellet, i.e., the orthorhombic phase, with a diameter and thickness of ~4.0 and ~1.3 mm, respectively. The obtained impedance spectra were fitted to electrical equivalent circuits and estimated bulk conductivities using the EC-Lab software (BioLogic). Above 270ºC, where the resistance is significantly reduced, the bulk contribution is outside the frequency range, so the conductivity (sum of bulk and grain boundary contributions) was estimated from the intercept of the spike (electrode component) and the real resistive axis.

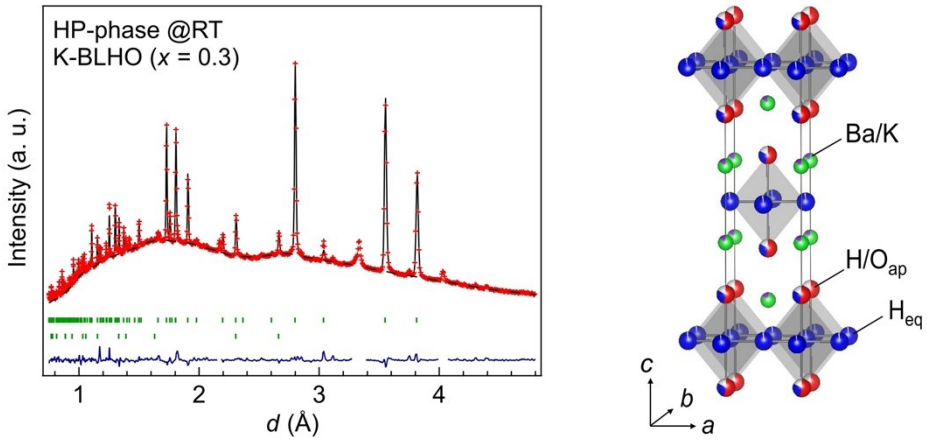

Fig. S1 Rietveld refinement profile of the ND data of K-BLHO (x = 0.3) synthesized via a high-pressure (HP) reaction, with the data collected at room temperature using the SPICA beamline. The final observed and calculated patterns are shown as red cross marks and black solid line, respectively. The blue solid line at the bottom of the plot represents the residual difference between the fitted and observed data. The green tick marks correspond to the positions of the Bragg reflections of the *I*4/*mmm* tetragonal phase (upper) and Li_2O (lower), respectively. The right-hand figure shows the refined crystal structure.

Table S1 Refined structural parameters of the high-pressure (HP) phase of K-BLHO (x = 0.3) at room temperature. The Li occupancies are fixed.

Phase 1: HP phase of K-BLHO (x = 0.3) (98 wt.%) refined: $K_{0.28(3)}Ba_{1.72(3)}LiH_{2.515(7)}O_{1.0708(11)}$

Atom	Site	g	x	y	z	B/Å^2
K/Ba	4*e*	1 – g(Ba)/0.86(2)	0	0	0.35939(3)	0.465(15)
Li	4*e*	0.5	0	0	0.0185(2)	2.14(7)
H_{eq}	4*c*	0.942(5)	0.5	0	0	1.06(2)
H_{ap}/O_{ap}	4*e*	0.3153(13)/0.5354(8)	0	0	0.17004(7)	0.37(3)

Space group *I*4/*mmm*, a = 3.956968(6) Å, c = 14.18990(6) Å;

R_{wp} = 0.85 %, R_p = 0.53 %, S = 5.41, R_B = 6.96 %, R_F = 9.02 %.

Phase 2: Li_2O (2 wt.%)

Atom	Site	g	x	y	z	B/Å^2
Li	8*c*	1	0.25	0.25	0.25	1
O	4*a*	1	0	0	0	1

Space group *Fm*–3*m*, a = 4.61199(2) Å

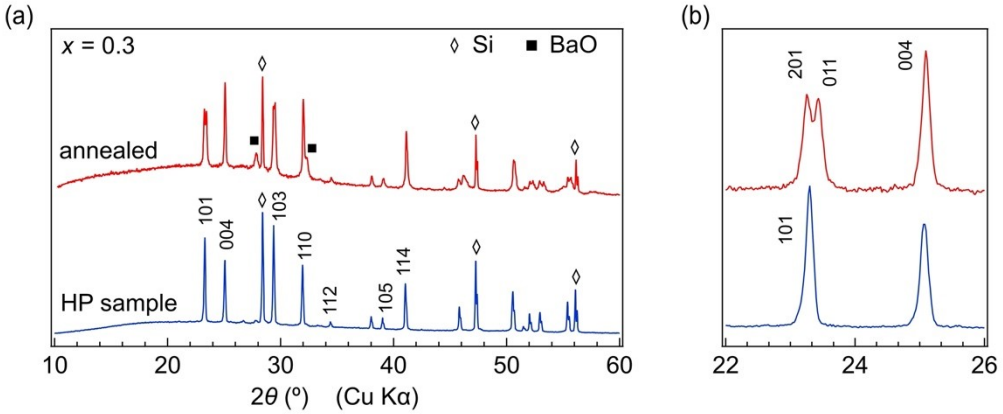

Fig. S2 (a) XRD patterns of the high-pressure (HP) sample of K-BLHO (x = 0.3) before and after annealing. BaO is formed via annealing, and Si is the internal standard reference. (b) Magnified XRD patterns showing the (101) and (004) reflections.

Structural refinements of the ambient-pressure phase of K-BLHO

Figures S3 and S5–7 and Tables S2–5 show the details of structural refinement and the refinement parameters of the annealed sample (x = 0.3), based on temperature-controlled ND data. The crystal structure at room temperature is similar to that of β-BLHO (space group: $Pnm2_1$), with three types of long-range order (H_{eq}/V_H, H_{ap}/O_{ap}, and Ba/V_{Ba}, Fig. S3 and Table S2). The crystal structure with x = 0.3 at 270 °C was refined using the same model as that used at room temperature, indicating that H_{eq}/V_H and Ba/V_{Ba} are disordered (Fig. S7 and Table S5). This suggests that the crystal structure with x = 0.3 at 270 °C resembles that of γ-BLHO (space group: *Pnma*). Thus, a structural refinement of the crystal structure with x = 0.3 at 270 °C was attempted using the same model as that of γ-BLHO, with a good fit obtained (Fig. S6 and Table S4). The crystal structure with x = 0.3 at 430 °C is the same simple K_2NiF_4-type structure (space group: *I*4/*mmm*) as that of δ-BLHO, and H^- and O^{2-} almost fully occupy the apical site (Fig. S5 and Table S3).

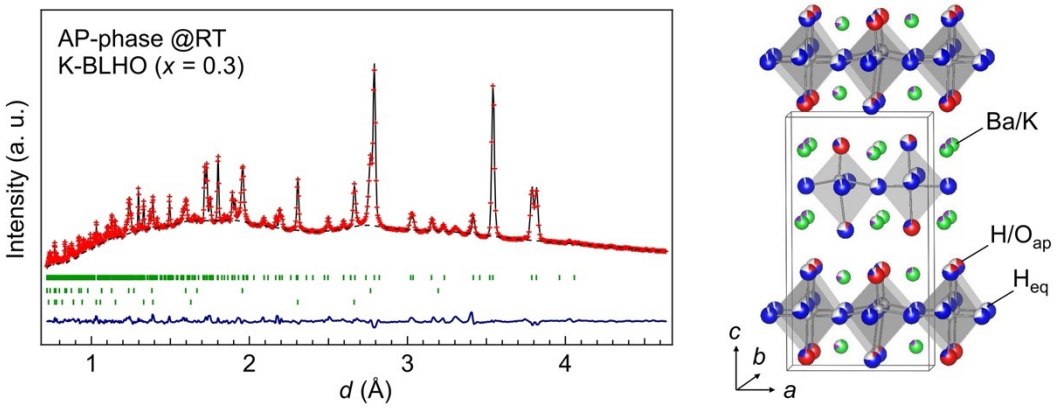

Fig. S3 Rietveld refinement profile of the ND data of the ambient-pressure (AP) phase of K-BLHO (x = 0.3) collected at room temperature using the SPICA beamline. The final observed and calculated patterns are shown as red cross marks and a black solid line, respectively. The blue solid line at the bottom of the plot represents the residual difference between the fitted and observed data. The green tick marks correspond to the positions of the Bragg reflections of the $Pnm2_1$ orthorhombic phase (upper), BaO (middle), and Li_2O (lower), respectively. The right-hand figure shows the refined crystal structure.

Table S2 Refined structural parameters of the ambient-pressure (AP) phase of K-BLHO (x = 0.3) at room temperature. The Li occupancies are fixed.

Phase 1: AP phase of K-BLHO (x = 0.3) at RT (73 wt.%) refined: $K_{0.297(3)}Ba_{1.465(2)}LiH_{2.476(6)}O_{0.9084\,(17)}$

Atom	Site	g	x	y	Z	B/Å^2
K/Ba1	2*a*	0.159(3)/0.8096(19)	0.1303(2)	0	0.86991(9)	0.237(8)
K/Ba2	2*a*	0.142(3)/0.6770(18)	0.6389(3)	0	0.58453(10)	= B(Ba1)
KBa3	2*a*	0.154(3)/0.811(2)	0.1105(3)	0	0.58409(9)	= B(Ba1)
KBa4	2*a*	0.138(3)/0.6421(18)	0.6185(3)	0	0.85802(11)	= B(Ba1)
Li1	2*a*	1	0.1465(5)	0	0.2179(3)	0.90(4)
Li2	2*a*	1	0.6470(5)	0	0.2431(2)	= B(Li1)
$H_{eq}1$	2*a*	0.722(4)	0.8817(3)	0	0.74796(14)	0.805(17)
$H_{eq}2$	2*a*	0.946(4)	0.3940(3)	0	0.72415(15)	= B($H_{eq}1$)
$H_{eq}3$	2*a*	0.947(5)	0.8785(4)	0	0.21769(14)	= B($H_{eq}1$)
$H_{eq}4$	2*a*	0.711(5)	0.3725(5)	0	0.2152(2)	= B($H_{eq}1$)
$H_{ap}/O_{ap}1$	2*a*	0.598(2)/0.2043(14)	0.1557(8)	0	0.3884(4)	0.30(6)
$H_{ap}/O_{ap}2$	2*a*	0.648(2)/0.1051(15)	0.6028(5)	0	0.0435(3)	= B($H_{ap}1$)
$H_{ap}/O_{ap}3$	2*a*	0.230(2)/0.7550(15)	0.1374(3)	0	0.05413(13)	0.206(18)
$H_{ap}/O_{ap}4$	2*a*	0.152(3)/0.7522(19)	0.6312(3)	0	0.37551(12)	= B($H_{ap}3$)

Space group $Pnm2_1$, a = 7.924549(14) Å, b = 3.929816(7) Å, c = 14.16475(4) Å;

R_{wp} = 1.14 %, R_p = 0.844 %, S = 21.8, R_B = 8.67 %, R_F = 8.76 %.

Phase 2: BaO (24 wt.%)

Atom	Site	g	x	y	z	B/Å^2
Ba	4*a*	1	0	0	0	0.5
O	4*b*	1	0.5	0.5	0.5	1

Space group $Fm\bar{3}m$, a = 5.532380(16) Å

Phase 3: Li_2O (3 wt.%)

Atom	Site	g	x	y	z	B/Å^2
Li	8*c*	1	0.25	0.25	0.25	1
O	4*a*	1	0	0	0	1

Space group $Fm\bar{3}m$, a = 4.612015(10) Å

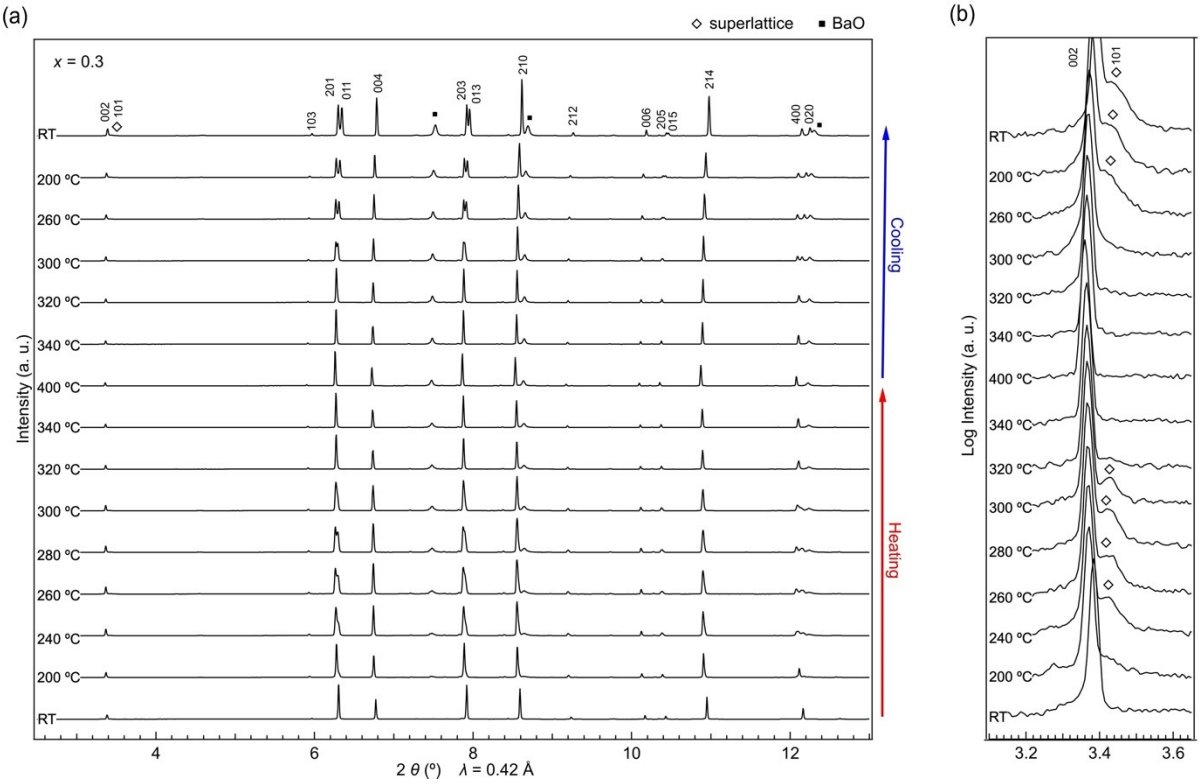

Fig. S4 (a) Temperature-controlled SXRD patterns of K-BLHO (x = 0.3). (b) Magnified patterns showing the (002) and (101) reflections.

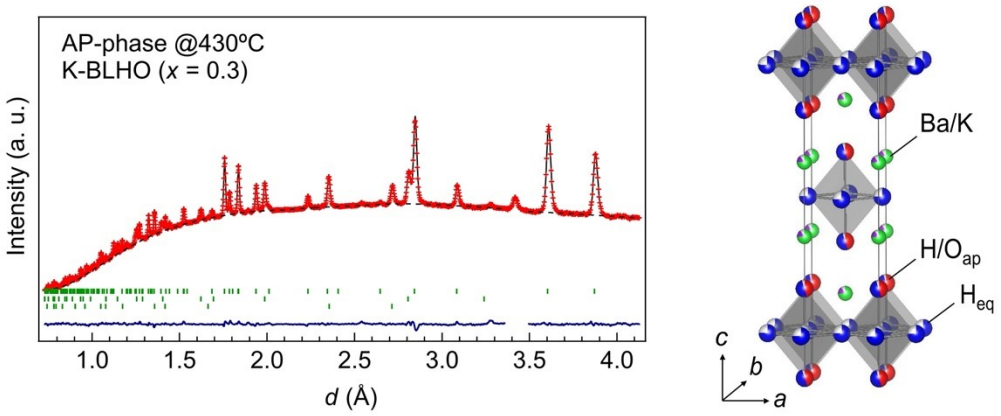

Fig. S5 Rietveld refinement profiles of the ND data of the ambient-pressure (AP) phase of K-BLHO (x = 0.3), with the data collected at 430 °C using the NOVA beamline. The final observed and calculated patterns are shown as red cross marks and a black solid line, respectively. The blue solid line at the bottom of the plot represents the residual difference between the fitted and observed data. The green tick marks correspond to the positions of the Bragg reflections of the *I*4/*mmm* tetragonal phase (upper), BaO (middle), and Li_2O (lower), respectively. The right-hand figure shows the refined crystal structure.

Table S3. Refined structural parameters of the ambient-pressure (AP) phase of K-BLHO (x = 0.3) at 430 °C. The Li occupancies are fixed.

Phase 1: AP phase of K-BLHO (x = 0.3) at 430 ºC (86 wt.%) refined: $K_{0.3}Ba_{1.5}LiH_{2.505(10)}O_{0.910(2)}$

Atom	Site	g	x	y	z	B/Å^2
K/Ba	4*e*	0.15/0.75	0	0	0.36112(8)	1.21(5)
Li	4*e*	0.5	0	0	0.0133(8)	3.23(10)
H_{eq}	4*c*	0.756(5)	0.5	0	0	2.26(8)
H_{ap}/O_{ap}	4*e*	0.4965(13)/0.4548(9)	0	0	0.1667(3)	0.73(14)

Space group *I*4/*mmm*, a = 3.98917(3) Å, c = 14.3158(2) Å;

R_{wp} = 0.83 %, R_p = 0.63 %, S = 2.03, R_B = 4.74 %, R_F = 6.20 %.

Phase 2: BaO (12 wt.%)

Atom	Site	g	x	y	z	B/Å^2
Ba	4*a*	1	0	0	0	0.5
O	4*b*	1	0.5	0.5	0.5	1

Space group *Fm*–3*m*, a = 5.57237(11) Å

Phase 3: Li_2O (2 wt.%)

Atom	Site	g	x	y	z	B/Å^2
Li	8*c*	1	0.25	0.25	0.25	1
O	4*a*	1	0	0	0	1

Space group *Fm*–3*m*, a = 4.66515(12) Å

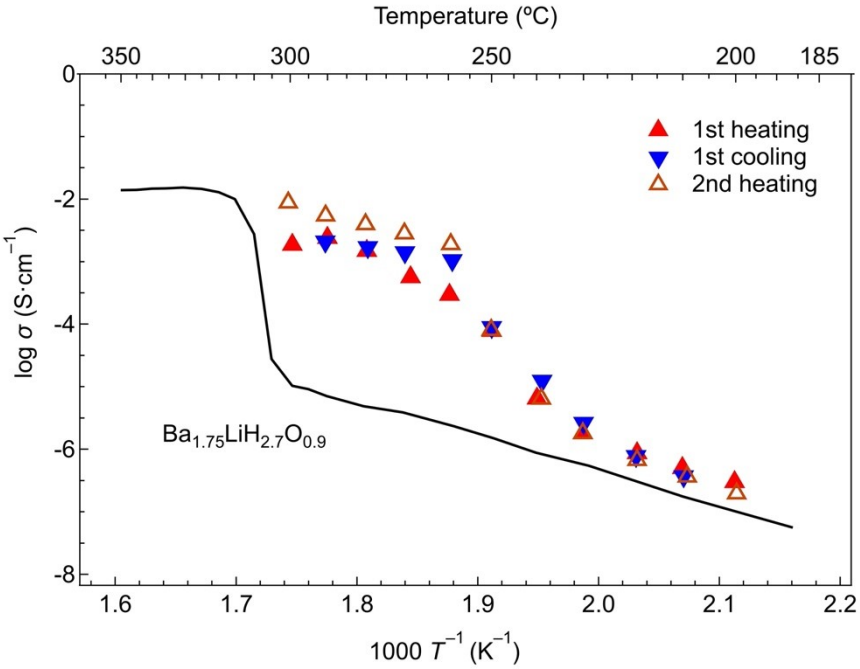

Fig. S6 The reversibility of the concavities for K-BLHO (x = 0.3) at 200 ≤ T ≤ 300 ºC .

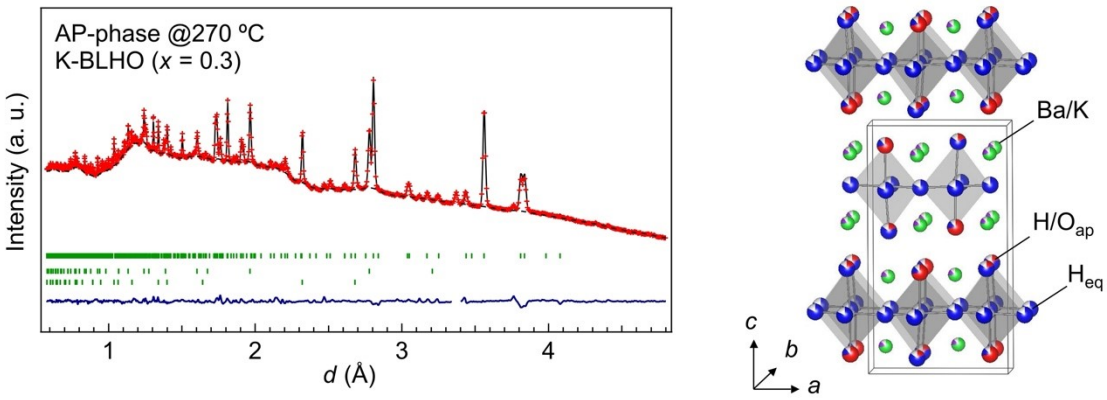

Fig. S7 Rietveld refinement profile of the ND data of the ambient-pressure (AP) phase of K-BLHO (x = 0.3) collected at 270 °C using the SPICA beamline. The final observed and calculated patterns are shown as red cross marks and a black solid line, respectively. The blue solid line at the bottom of the plot represents the residual difference between the fitted and observed data. The green tick marks correspond to the positions of the Bragg reflections of the *Pnma* orthorhombic phase (upper), BaO (middle), and Li_2O (lower), respectively. The right-hand figure shows the refined crystal structure.

Table S4 Refined structural parameters of the AP phase of K-BLHO (x = 0.3) at 270 °C.

Phase 1: AP phase of K-BLHO (x = 0.3) at 270 ºC (72 wt.%) refined: $K_{0.302(7)}Ba_{1.456(6)}LiH_{2.466(11)}O_{0.907(4)}$

Atom	Site	g	x	y	z	B/Å^2
K/Ba1	4c	0.150(7)/0.723(5)	0.1143(7)	0.25	0.1058(2)	0.29(4)
K/Ba2	4c	0.152(7)/0.733(5)	0.1343(7)	0.25	0.38674(18)	= B(Ba1)
Li	4c	1	0.380(3)	0.75	0.2501(8)	3.06(18)
$H_{eq}1$	4c	0.819(8)	0.3603(11)	0.25	0.2456(3)	1.44(7)
$H_{eq}2$	4c	0.824(9)	0.1307(15)	0.75	0.2444(4)	= B($H_{eq}1$)
$H_{ap}/O_{ap}1$	4c	0.664(4)/0.185(2)	0.359(2)	0.75	0.0699(7)	1.1(3)
$H_{ap}/O_{ap}2$	4c	0.159(6)/0.722(4)	0.3809(8)	0.75	0.4127(2)	0.55(9)

Space group *Pnma*, a = 7.96493(9) Å, b = 3.95435(4) Å, c = 14.2442(2) Å;

R_{wp} = 0.68 %, R_p = 0.47 %, S = 3.99, R_B = 9.82 %, R_F = 9.57 %.

Phase 2: BaO (23 wt.%)

Atom	Site	g	x	y	z	B/Å^2
Li	4a	1	0	0	0	0.5
O	4a	1	0.5	0.5	0.5	1

Space group *Fm*–3*m*, a = 5.55581(9) Å

Phase 3: Li_2O (5 wt.%)

Atom	Site	g	x	y	z	B/Å^2
Li	8c	1	0.25	0.25	0.25	1
O	4a	1	0	0	0	1

Space group *Fm*–3*m*, a = 4.64247(8) Å

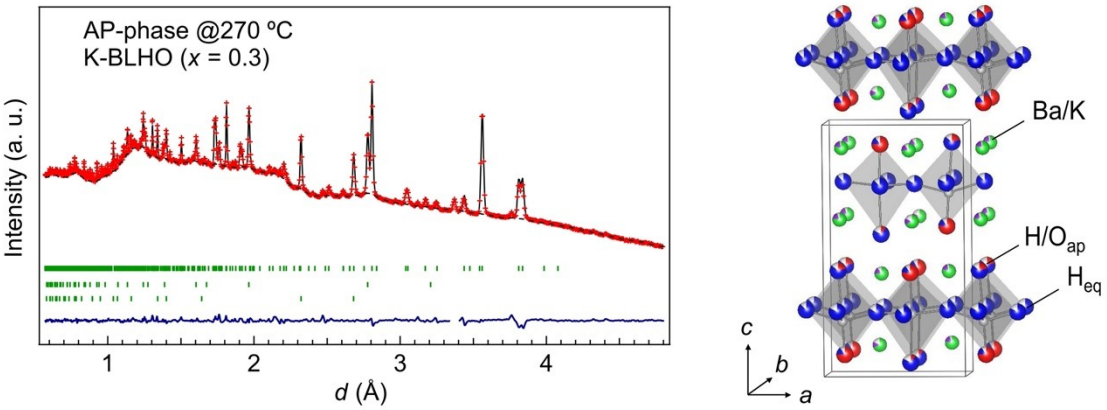

Fig. S8 Rietveld refinement profiles of the ND data of the ambient-pressure (AP) phase of K-BLHO (x = 0.3) collected at 270 °C using the SPICA beamline. The final observed and calculated patterns are shown as red cross marks and a black solid line, respectively. The blue solid line at the bottom of the plot represents the residual difference between the fitted and observed data. The green tick marks correspond to the positions of the Bragg reflections of the $Pnm2_1$ orthorhombic phase (upper), BaO (middle), and Li_2O (lower), respectively. The right-hand figure shows the refined crystal structure.

Table S5. Refined structural parameters of the ambient-pressure (AP) phase of K-BLHO (x = 0.3) at 270 °C. The Li occupancies are fixed.

Phase 1: AP phase of K-BLHO (x = 0.3) at 270 ºC (70 wt.%) refined: $K_{0.293(11)}Ba_{1.510(8)}LiH_{2.55(3)}O_{0.910(6)}$

Atom	Site	g	x	y	z	B/Å^2
K/Ba1	2*a*	0.157(13)/0.801(10)	0.1366(8)	0	0.9089(4)	0.34(3)
K/Ba2	2*a*	0.132(12)/0.683(8)	0.6315(11)	0	0.6167(5)	= B(Ba1)
KBa3	2*a*	0.157(12)/0.782(9)	0.1197(10)	0	0.6247(3)	= B(Ba1)
KBa4	2*a*	0.139(12)/0.753(8)	0.6135(9)	0	0.8997(4)	= B(Ba1)
Li1	2*a*	1	0.133(3)	0	0.2199(8)	2.9(2)
Li2	2*a*	1	0.625(4)	0	0.2488(10)	= B(Li1)
$H_{eq}1$	2*a*	0.83(2)	0.8776(17)	0	0.7692(10)	1.49(6)
$H_{eq}2$	2*a*	0.88(3)	0.4073(11)	0	0.7569 (8)	= B($H_{eq}1$)
$H_{eq}3$	2*a*	0.88(3)	0.8781(15)	0	0.2656(10)	= B($H_{eq}1$)
$H_{eq}4$	2*a*	0.83(3)	0.374(2)	0	0.2562(8)	= B($H_{eq}1$)
$H_{ap}/O_{ap}1$	2*a*	0.654(8)/0.208(5)	0.106(3)	0	0.4213(15)	0.59(16)
$H_{ap}/O_{ap}2$	2*a*	0.726(9)/0.103(6)	0.614(2)	0	0.0560(6)	= B($H_{ap}1$)
$H_{ap}/O_{ap}3$	2*a*	0.146(11)/0.757(7)	0.1478(9)	0	0.0881(4)	0.31(8)
$H_{ap}/O_{ap}4$	2*a*	0.150(11)/0.752(7)	0.6156(9)	0	0.4129(4)	= B($H_{ap}3$)

Space group $Pnm2_1$, a = 7.96630(6) Å, b = 3.95473(3) Å, c = 14.24362(10) Å;

R_{wp} = 0.65 %, R_p = 0.44 %, S = 3.84, R_B = 9.41 %, R_F = 8.11 %.

Phase 2: BaO (25 wt.%)

Atom	Site	g	x	y	z	B/Å^2
Ba	4*a*	1	0	0	0	0.5
O	4*b*	1	0.5	0.5	0.5	1

Space group *Fm*–3*m*, a = 5.55570(5) Å

Phase 3: Li_2O (5 wt.%)

Atom	Site	g	x	y	z	B/Å^2
Li	8*c*	1	0.25	0.25	0.25	1
O	4*a*	1	0	0	0	1

Space group *Fm*–3*m*, a = 4.64302(3) Å

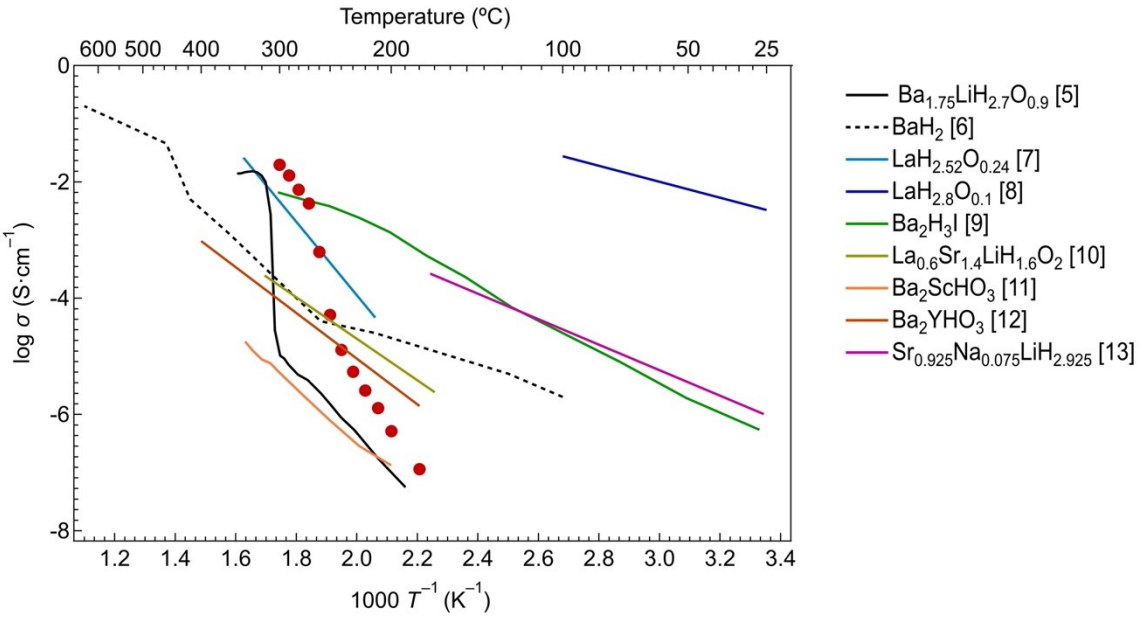

Fig. S9 Comparison of conductivities of reported H^- conductors; $Ba_{1.75}LiH_{2.7}O_{0.9}$[5], BaH_2[6], $LaH_{3-2x}O_x$ (x = 0.1[7], 0.24[8]), Ba_2H_3I[9], $La_{0.6}Sr_{1.4}LiH_{1.6}O_2$[10], Ba_2ScHO_3[11], Ba_2YHO_3[12], $Sr_{0.925}Na_{0.075}LiH_{2.925}$[13].

References

1. S. Kawaguchi, M. Takemoto, K. Osaka, E. Nishibori, C. Moriyoshi, Y. Kubota, Y. Kuroiwa and K. Sugimoto, *Rev. Sci. Instrum.*, 2017, **88**, 085111.
2. F. Izumi and K. Momma, *Solid State Phenomena*, 2007, **130**, 15-20.
3. R. Oishi, M. Yonemura, Y. Nishimaki, S. Torii, A. Hoshikawa, T. Ishigaki, T. Morishima, K. Mori and T. Kamiyama, *Nuclear Instruments & Methods in Physics Research Section a-Accelerators Spectrometers Detectors and Associated Equipment*, 2009, **600**, 94-96.
4. K. Momma and F. Izumi, *J. Appl. Crystallogr.*, 2011, **44**, 1272-1276.
5. F. Takeiri, A. Watanabe, K. Okamoto, D. Bresser, S. Lyonnard, B. Frick, A. Ali, Y. Imai, M. Nishikawa, M. Yonemura, T. Saito, K. Ikeda, T. Otomo, T. Kamiyama, R. Kanno and G. Kobayashi, *Nat. Mater.*, 2022, **21**, 325-330.
6. M. C. Verbraeken, C. Cheung, E. Suard and J. T. Irvine, *Nat. Mater.*, 2015, **14**, 95-100.
7. K. Fukui, S. Iimura, T. Tada, S. Fujitsu, M. Sasase, H. Tamatsukuri, T. Honda, K. Ikeda, T. Otomo and H. Hosono, *Nat. Commun.*, 2019, **10**, 2578.
8. K. Fukui, S. Iimura, A. Iskandarov, T. Tada and H. Hosono, *J. Am. Chem. Soc.*, 2022, **144**, 1523-1527.
9. H. Ubukata, F. Takeiri, C. Tassel, S. Kobayashi, S. Kawaguchi, T. Saito, T. Kamiyama, S. Kobayashi, G. Kobayashi and H. Kageyama, *Chem. Mater.*, 2022.
10. G. Kobayashi, Y. Hinuma, S. Matsuoka, A. Watanabe, M. Iqbal, M. Hirayama, M. Yonemura, T.

Kamiyama, I. Tanaka and R. Kanno, *Science*, 2016, **351**, 1314-1317.

11. F. Takeiri, A. Watanabe, A. Kuwabara, H. Nawaz, N. I. P. Ayu, M. Yonemura, R. Kanno and G. Kobayashi, *Inorg. Chem.*, 2019, **58**, 4431-4436.
12. H. Nawaz, F. Takeiri, A. Kuwabara, M. Yonemura and G. Kobayashi, *Chem. Commun.*, 2020, **56**, 10373-10376.
13. T. Hirose, T. Mishina, N. Matsui, K. Suzuki, T. Saito, T. Kamiyama, M. Hirayama and R. Kanno, *ACS Appl. Energy Mater.*, 2022, **5**, 2968-2974.